Localization effects in mixed-ligand gold bis(dithiolene) complexes as single component conductors

Haia Kharraz,[a] Pere Alemany,[b] Enric Canadell,*[c,d] Antoine Vacher,[a] Thierry Roisnel,[a] Hengbo Cui,[e] Kee Hoon Kim,[e] Marc Fourmigué*[a] and Dominique Lorcy*[a]

SUPPLEMENTARY MATERIAL

Table S1 Bond lengths (in Å) in the monoanionic and neutral complexes, and reference TMTTF and $TMTTF^{+\bullet}$ salt

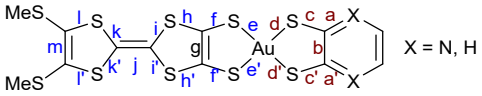

	[Au(BMT-TTF)(pzdt)]$^{-1}$	[Au(BMT-TTF)(pzdt)]•	[Au(EDT-TTF)(bdt)]$^{-1}$	[Au(BMT-TTF)(bdt)]$^{-1}$	[Au(BMT-TTF)(bdt)]•	$TMTTF^{0}$	$(TMTTF^{+\bullet})(FeCl_4)$
a	1.336(4)	1.333(5)	1.406(15)	1.388(12)	1.410(18)		
a’	1.330(4)	1.335(5)	1.389(15)	1.388(14)	1.398(19)		
b	1.417(4)	1.405(5)	1.419(14)	1.390(12)	1.427(19)		
c	1.748(3)	1.750(4)	1.741(11)	1.761(8)	1.753(13)		
c’	1.749(3)	1.746(4)	1.748(10)	1.767(8)	1.744(14)		
d	2.3141(8)	2.3045(10)	2.297(3)	2.320(3)	2.296(3)		
d’	2.3112(8)	2.3009(10)	2.293(2)	2.303(4)	2.291(3)		
e	2.3153(8)	2.3374(9)	2.317(2)	2.334(3)	2.329(3)		
e’	2.3224(8)	2.3204(10)	2.325(3)	2.326(3)	2.323(3)		
f	1.744(3)	1.728(4)	1.745(10)	1.807(13)	1.729(13)	1.777(3)	1.728(8)
f’	1.744(3)	1.732(4)	1.771(10)	1.788(14)	1.737(13)	1.697(2)	1.740(8)
g	1.341(4)	1.361(5)	1.292(14)	1.199(17)	1.332(19)	1.261(3)	1.362(13)
h	1.770(3)	1.742(4)	1.764(10)	1.796(14)	1.733(12)	1.720(2)	1.725(7)
h’	1.769(3)	1.733(4)	1.763(10)	1.774(13)	1.738(13)	1.760(2)	1.745(8)
i	1.761(3)	1.729(4)	1.770(11)	1.743(13)	1.733(13)	1.672(2)	1.722(10)
i’	1.760(3)	1.735(4)	1.788(9)	1.789(14)	1.718(12)	1.687(2)	1.719(8)
j	1.343(4)	1.375(5)	1.229(16)	1.332(19)	1.384(16)	1.348(3)	1.380(9)
k	1.763(3)	1.730(4)	1.789(9)	1.759(14)	1.736(13)	1.678(2)	1.691(8)
k’	1.752(3)	1.723(4)	1.811(11)	1.746(12)	1.729(12)	1.669(2)	1.738(10)
l	1.761(3)	1.740(4)	1.755(11)	1.757(16)	1.755(14)	1.703(2)	1.734(6)
l’	1.756(3)	1.744(4)	1.756(10)	1.767(16)	1.754(14)	1.763(2)	1.736(8)
m	1.348(4)	1.357(5)	1.362(15)	1.358(19)	1.324(19)	1.255(3)	1.343(13)

(a) From ref 1. (b) From ref. 2, in its $FeCl_4^-$ salt.

Table S2 Crystallographic data[a,b]

	[*n*-Bu$_4$N][Au(EDT-TTFS$_2$)(bdt)]	**[*n*-Bu$_4$N][Au(BMT-TTFS$_2$)(pzdt)]**	**[Au(BMT-TTFS$_2$)(pzdt)]$^{\bullet}$**	**[*n*-Bu$_4$N][Au(BMT-TTFS$_2$)(bdt)]**	**[Au(BMT-TTFS$_2$)(bdt)]$^{\bullet}$**	**(*n*-Bu$_4$N)(TCNQ)$_3$**
CCDC	2474551	2474552	2474553	2474554	2474555	2474556
Formulae	$C_{30}H_{44}AuNS_{10}$	$C_{28}H_{44}AuN_3S_{10}$	$C_{12}H_8AuN_2S_{10}$	$C_{30}H_{46}AuNS_{10}$	$C_{14}H_{10}AuS_{10}$	$C_{52}H_{48}N_{13}$
FW (g.mol^{-1})	936.23	940.23	697.77	938.24	695.79	855.03
System	monoclinic	triclinic	monoclinic	monoclinic	triclinic	triclinic
Space group	$P2_1/c$	$P\bar{1}$	$P2_1/c$	$C2/c$	$P\bar{1}$	$P1$
a (Å)	23.223(4)	10.4576(11)	7.4349(8)	36.911(9)	7.7151(14)	7.9061(12)
b (Å)	8.5098(11)	12.8379(13)	34.610(4)	16.520(4)	8.9038(15)	9.8893(14)
c (Å)	19.322(3)	14.4741(14)	7.9273(8)	12.564(3)	15.024(3)	16.027(2)
α (deg)	90	86.550(4)	90	90	101.512(7)	73.825(5)
β (deg)	107.283(5)	78.376(4)(5)	107.325(4)	98.429(5)	90.352(7)	79.606(6)
γ (deg)	90	73.963(4)	90	90	104.565(6)	80.314(6)
V (Å^3)	3646.0(9)	1829.3(3)	1947.3(4)	7579(3)	977.0(3)	1174.5(3)
T (K)	150(2)	150(2)	150(2)	150(2)	150(2)	150(2)
Z	4	2	4	8	2	1
D_{calc} (g.cm^{-3})	1.706	1.707	2.380	1.645	2.365	1.209
μ (mm^{-1})	4.631	4.617	8.628	4.456	8.595	0.075
Total refls	30306	28355	29642	30389	3827	11938
Abs corr	multi-scan	multi-scan	multi-scan	multi-scan	multi-scan	multi-scan
Uniq refls (R_{int})	7379(0.0831)	8374(0.0331)	4461(0.0421)	8881(0.1026)	3827	8394 (0.033)
Uniq refls (I > 2σ(I))	6085	7745	4172	5501	3163	6112
R_1, wR_2	0.0687,0.1599	0.0245, 0.0571	0.0255, 0.0438	0.0847, 0.1600	0.0580, 0.1322	0.0896, 0.2396
R_1, wR_2 (all data)	0.0863,0.1704	0.0284, 0.0592	0.0288, 0.0446	0.1423, 0.1858	0.0778, 0.1414	0.1176, 0.2664
GOF	1.076	0.949	1.195	1.050	1.093	1.049

[a] $R_1 = ||F_o| - |F_c||/|F_o|$. [b] $wR_2 = [w(F_o^2 - F_c^2)^2]/[w(F_{o2})^2]^{1/2}$.

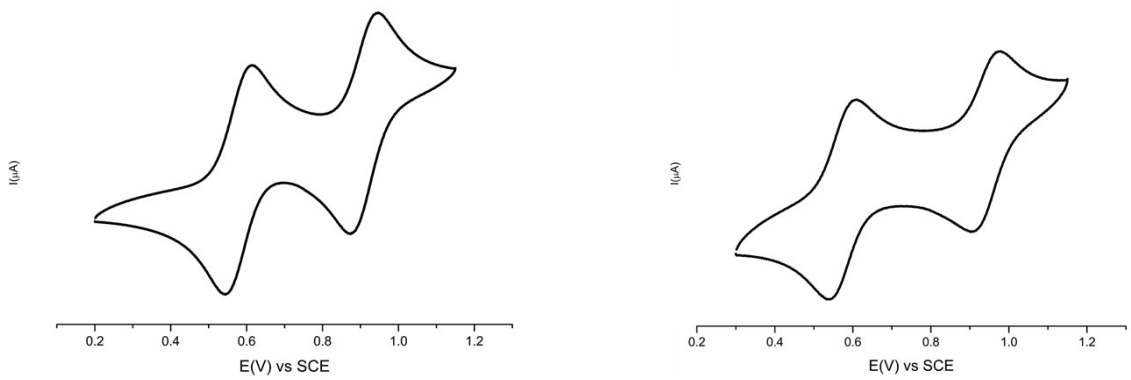

Fig. S1 Cyclic voltammograms of TTF **1** (left, $E^1_{1/2}$ = 0.58 V and $E^2_{1/2}$ = 0.91 V vs SCE) and TTF **2** (right, $E^1_{1/2}$ = 0.58 V and $E^2_{1/2}$ = 0.94 V vs SCE) performed in CH_2Cl_2.

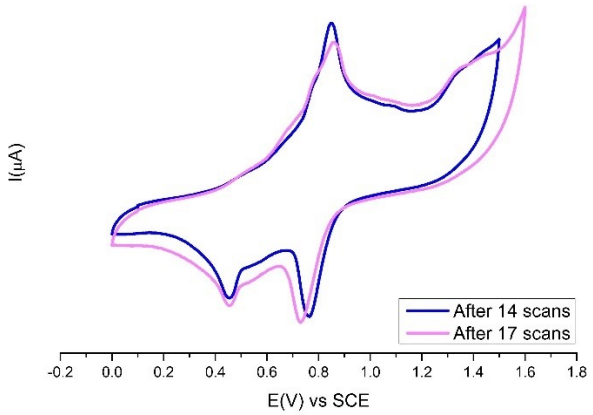

Fig. S2 Cyclic voltammograms of $[Au(BMT\text{-}TTFS_2)(pzdt)]^{-1}$ in CH_3CN using 0.1M of $[Bu_4N][PF_6]$ after 14 and 17 scans.

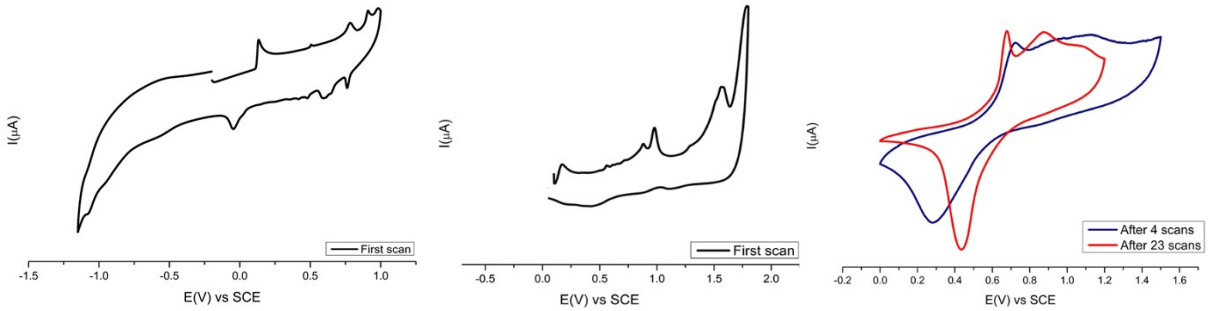

Fig. S3 Cyclic voltammograms of $[Au(BMT\text{-}TTFS_2)(bdt)]^{-1}$ in CH_3CN (left) and in CH_2Cl_2 (middle) using 0.1M of $[Bu_4N][PF_6]$ and (right) evolution of the CVs upon several scans in CH_2Cl_2.

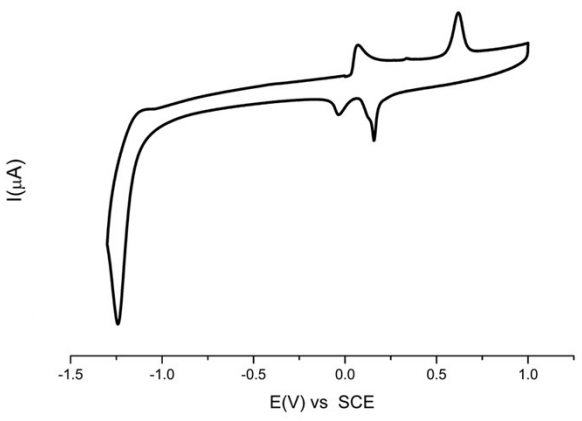

Fig. S4 Cyclic voltammogram of $[Au(EDT\text{-}TTFS_2)(bdt)]^{-1}$ performed in CH_2Cl_2 using 0.1M of $[Bu_4N][PF_6]$.

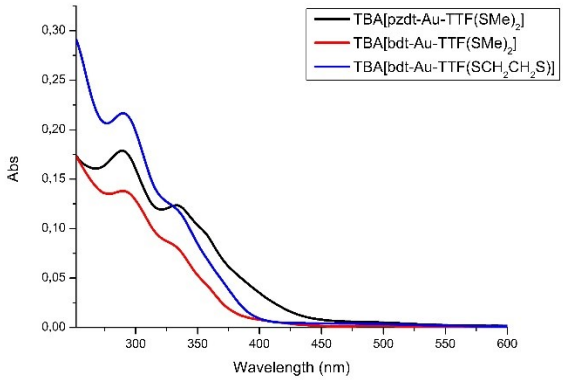

Fig. S5 UV-vis absorption spectra of the three monoanionic complexes

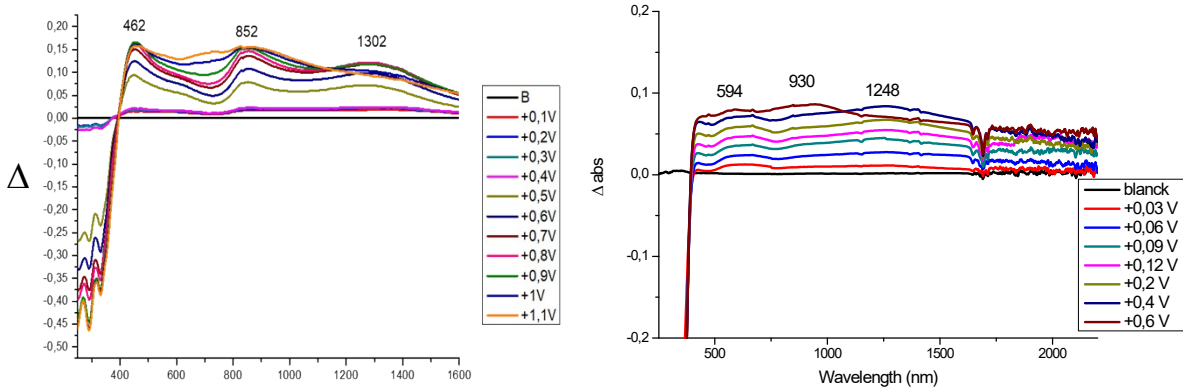

Fig. S6 UV-vis-NIR monitoring of the electrochemical oxidation of the monoanionic complexes in CH_2Cl_2, left : [*n*-Bu_4N][$Au(BMT\text{-}TTFS_2)(pzdt)$] and right: [*n*-$Bu_4N$][$Au(EDT\text{-}TTFS_2)(bdt)$]. The higher insolubility of the latter complex is visible from the less visible absorption bands.

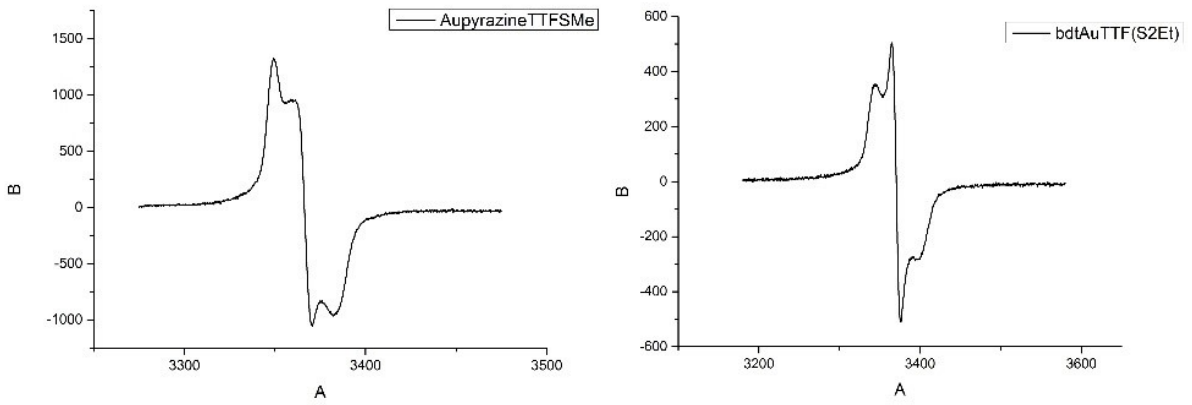

Fig. S7 X-band EPR spectra of polycrystalline samples of [Au(BMTTTFS$_2$)(pzdt)]$^{\bullet}$ (left) and [Au(EDT-TTFS$_2$)(bdt)]$^{\bullet}$ (right).

(a)

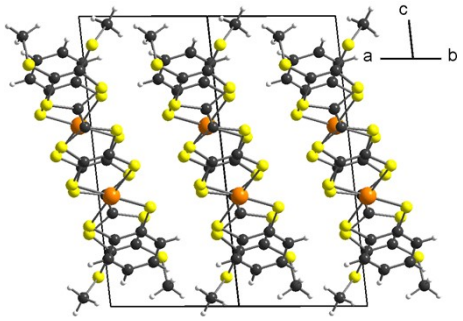

(b)

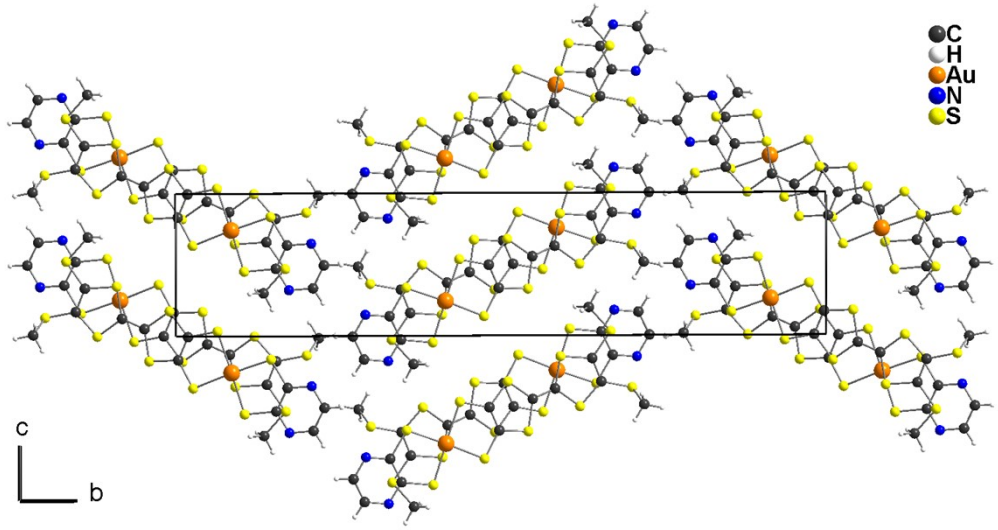

Fig. S8 Structural organization of (a) [Au(BMT-TTFS$_2$)(bdt)]$^{\bullet}$ and (b) [Au(BMT-TTFS$_2$)(pzdt)]$^{\bullet}$.

Table S3 Evolution of transport properties at room temperature in [Au(BMT-TTFS$_2$)(bdt)]$^{\bullet}$.

Pressure (GPa)	Resistivity (Ω cm)	Activation energy (meV)	Conductivity (S cm^{-1})
1.0	14 239	112	7×10^{-5}
1.8	3 694	235	2.7×10^{-4}
2.6	1 442	267	7×10^{-4}
3.8	315	249	3×10^{-3}
5.1	58	153	0.017
6.4	5	77	0.19

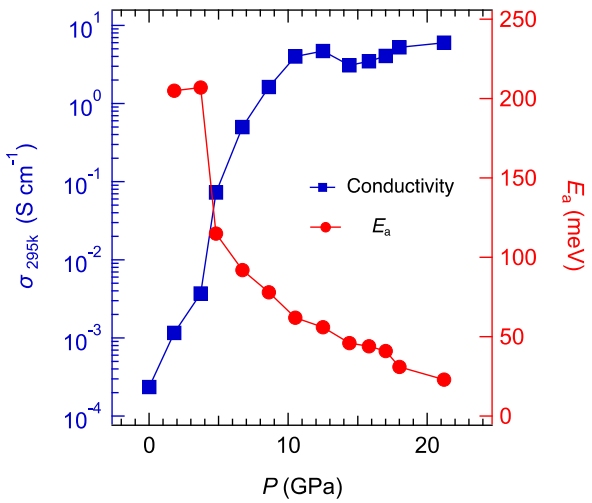

Fig. S9 Evolution of transport properties at room temperature in [Au(BMT-TTFS$_2$)(pzdt)]$^{\bullet}$.

Table S4 Evolution of transport properties at room temperature in [Au(BMT-TTFS$_2$)(pzdt)]$^{\bullet}$.

Pressure (GPa)	Resistivity (Ω cm)	Activation Energy (meV)	Conductivity (S/cm)
1bar	7005.2		0.00014
1.8	860.7	205	0.0012
3.7	270.5	207	0.0037
4.8	13.7	115	0.073
6.7	2	92	0.5
8.6	0.61	78	1.6
10.5	0.25	62	4
12.5	0.21	56	4.7
14.4	0.32	46	3.1
15.8	0.29	44	3.5
17	0.25	41	4.1
18	0.19	31	5.3
21.2	0.17	23	6

Chemical attempt to form the neutral complex and details on the (*n*-Bu$_4$N)(TCNQ)$_3$ salt

Considering the low oxidation potential of the three complexes (0.12 – 0.20 V *vs.* SCE), we first attempted the oxidation of the monoanionic complex [*n*-Bu$_4$N][Au(BMT-TTFS$_2$)(bdt)] by using TCNQ as an oxidizing agent (E_{red} = +0.17 V *vs*. SCE). Black crystals were isolated together with an insoluble black powder. The crystals were analyzed as a mixed-valence salt of the reduced TCNQ, formulated as [Bu$_4$N][TCNQ]$_3$ with an original, unknown 1:3 stoichiometry. Investigation of the remaining insoluble powder by IR did not reveal any nitrile stretching vibration indicating that a redox reaction had occurred between the TCNQ and the monoanionic complex and that the insoluble powder was the neutral complex. The salt crystallizes in the triclinic system, space group *P*1, with one *n*-Bu$_4$N$^+$ and three TCNQ moieties in general position in the unit cell. The TCNQ molecules stack along the *b* axis, as shown in Figs. S9 and S10. Calculations of partial charges on the three TCNQs (Table S5), based on the Kistenmacher formulae,[3] show that TCNQ_A is essentially neutral while the two other TCNQ share the −1 charge. These values should be taken with care as the overall precision of the structure is not at the highest standard, with an averaged C–C bond precision of 0.0101 Å.

Overlap patterns (Fig. S11) are all of the bond-over-ring type, with however differences on the averaged plane-to-plane distances. Altogether the salt can be described as mixed-valence monoanionic BC dyads, alternating with essentially neutral A molecules.

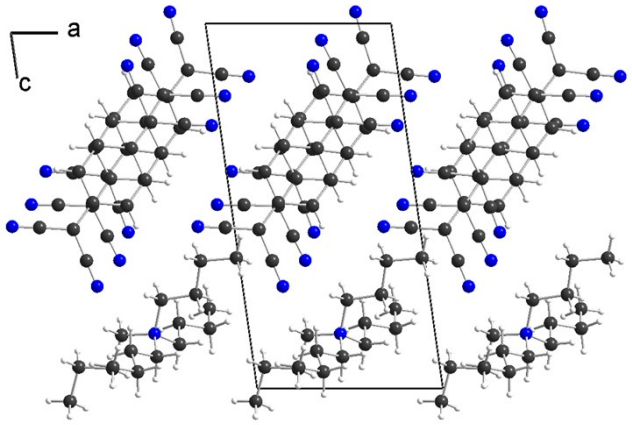

Fig. S10 Projection view along the stacking *b* axis of the unit cell of (*n*-Bu_4N)$(TCNQ)_3$ salt.

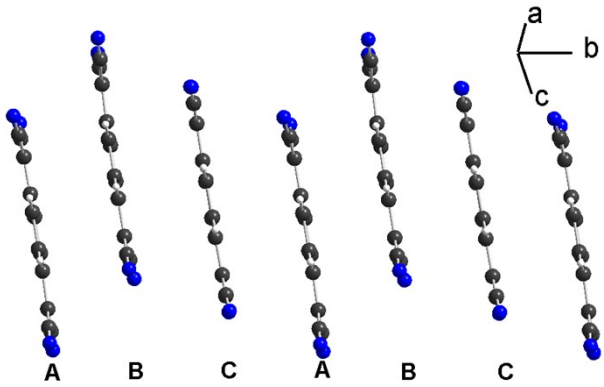

Fig. S11 Detail of the TCNQ stack in (*n*-Bu_4N)$(TCNQ)_3$ salt

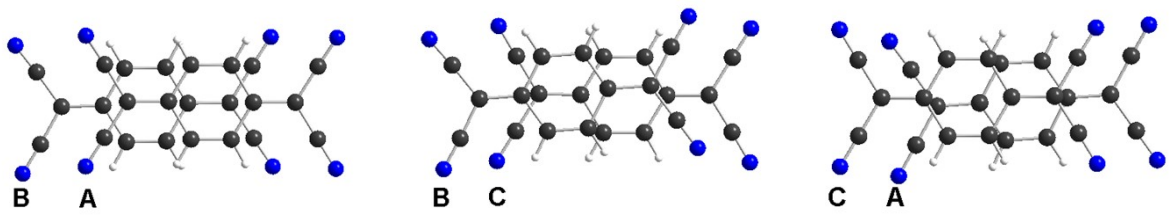

Plane-to-plane dist. 3.15 Å 3.26 Å 3.33 Å

Fig S12 Overlap patterns between TCNQs in (*n*-Bu_4N)$(TCNQ)_3$ salt

Table S5 Averaged bond distances within the three TCNQs. The estimated TCNQ charge (ρ_{calc}) is calculated according to the Kistenmacher formula which reads as $\rho_{TCNQ} = A[c/(b+d)] + B$, with $A_{TCNQ} = -41.667$ and $B_{TCNQ} = 19.833$, where a–d are averaged distances.

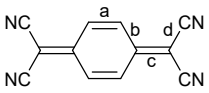

TCNQ	a (Å)	b (Å)	c (Å)	d (Å)	c/(b+d)	ρ_{calc}
TCNQ_A	1.356(10)	1.438(10)	1.389(10)	1.428(10)	0.4760	≈ 0
TCNQ_B	1.356(10)	1.427(10)	1.399(10)	1.428(10)	0.4900	−0.58
TCNQ_C	1.351(10)	1.437(10)	1.383(10)	1.431(10)	0.4822	−0.26

REFERENCES

[1] L. Wang, J. P. Zhang and B. Zhang, *Acta Crystallogr*., 2005, **E61**, 65–66.

[2] H. Endres, *Acta Crystallogr*., 1987, **C43**, 439–441.

[3] T. J. Kistenmacher, T. J. Emge, A. N. Bloch and D. O. Cowan, *Acta. Cryst. B*, 1982, **38**, 1193–1199.

DFT results for [Au(BMT-TTFS$_2$)(pzdt)]$^{\bullet}$

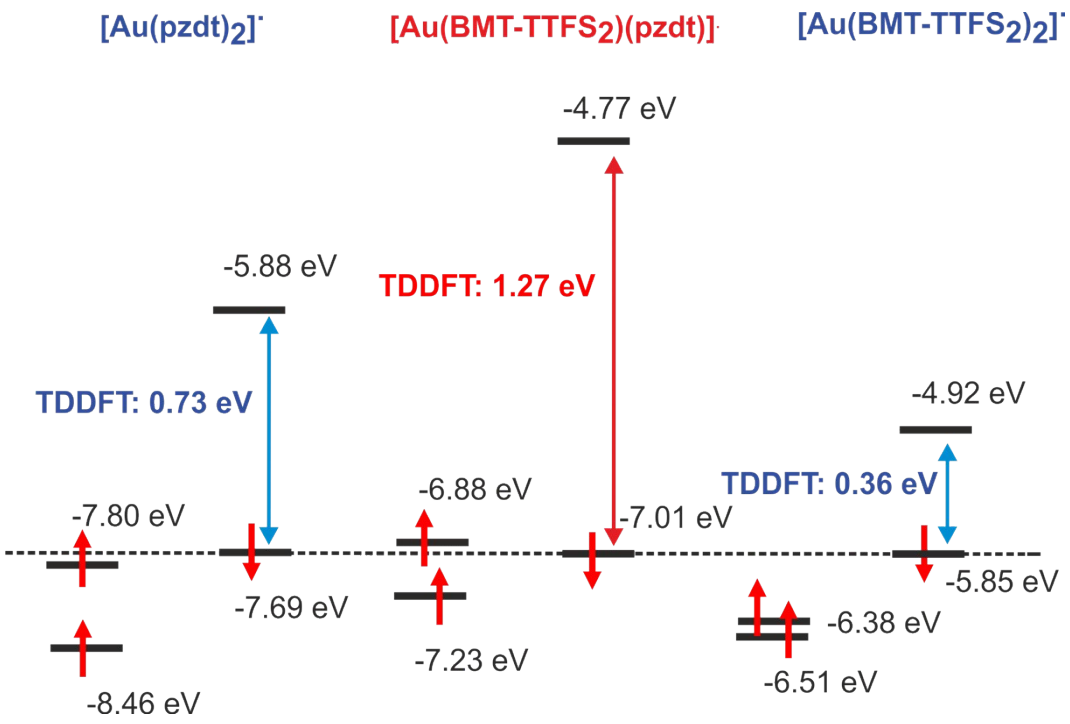

Fig. S13 [Au(BMT-TTFS$_2$)(pzdt)]$^{\bullet}$ complex: SOMO, SOMO–1 and LUMO levels and first significant low energy transition (SOMO–1→LUMO) as calculated by TDDFT for the asymmetric and the two associated symmetric complexes. Note that the energy of the β SOMO–1 levels of the three compounds have been aligned to obtain a clearer visual representation.

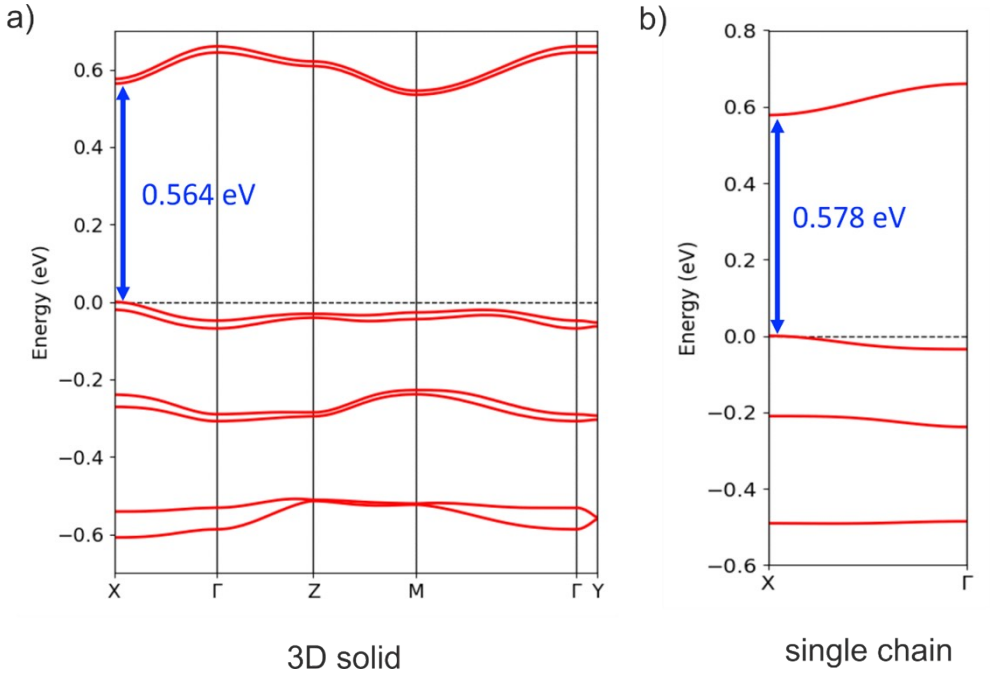

Fig. S14 Calculated band structure for: (a) 3D [Au(BMT-TTFS$_2$)(pzdt)]$^{\bullet}$, and (b) an isolated [Au(BMT-TTFS$_2$)(pzdt)]$^{\bullet}$ chain assuming double occupation of the levels. The dashed line refers to the highest occupied level and Γ= (0, 0, 0), X= (*a**/2, 0, 0), Y= (0, *b**/2, 0), M= (*a**/2, *b**/2, 0) and Z= (0, 0, *c**/2), respectively.